

# The surface structure of concentrated aqueous salt solutions

E. Sloutskin

*Department of Physics, Bar-Ilan University, Ramat-Gan 52900, Israel*

J. Baumert<sup>a)</sup> and B. M. Ocko

*Department of Soft Condensed Matter and Materials Science, Brookhaven National Laboratory, Upton, New York 11973*

I. Kuzmenko

*CMC-CAT, Advanced Photon Source, Argonne National Laboratory, Illinois 60439*

A. Checco

*Department of Soft Condensed Matter and Materials Science, Brookhaven National Laboratory, Upton, New York 11973*

L. Tamam and E. Ofer

*Department of Physics, Bar-Ilan University, Ramat-Gan 52900, Israel*

T. Gog

*CMC-CAT, Advanced Photon Source, Argonne National Laboratory, Illinois 60439*

O. Gang

*Department of Soft Condensed Matter and Materials Science, Brookhaven National Laboratory, Upton, New York 11973*

M. Deutsch<sup>b)</sup>

*Department of Physics, Bar-Ilan University, Ramat-Gan 52900, Israel*

(Received 23 August 2006; accepted 7 December 2006; published online 2 February 2007)

The surface-normal electron density profile  $\rho_s(z)$  of concentrated aqueous salt solutions of RbBr, CsCl, LiBr, RbCl, and SrCl<sub>2</sub> was determined by x-ray reflectivity (XR). For all but RbBr and SrCl<sub>2</sub>  $\rho_s(z)$  increases monotonically with depth  $z$  from  $\rho_s(z)=0$  in the vapor ( $z<0$ ) to  $\rho_s(z)=\rho_b$  of the bulk ( $z>0$ ) over a width of a few angstroms. The width is commensurate with the expected interface broadening by thermally excited capillary waves. Anomalous (resonant) XR of RbBr reveals a depletion at the surface of Br<sup>-</sup> ions to a depth of  $\sim 10$  Å. For SrCl<sub>2</sub>, the observed  $\rho_s(z) > \rho_b$  may imply a similar surface depletion of Cl<sup>-</sup> ions to a depth of a few angstroms. However, as the deviations of the XRs of RbBr and SrCl<sub>2</sub> from those of the other solutions are small, the evidence for a different ion composition in the surface and the bulk is not strongly conclusive. Overall, these results contrast earlier theoretical and simulational results and nonstructural measurements, where significant surface layering of alternate, oppositely charged, ions is concluded. © 2007 American Institute of Physics. [DOI: [10.1063/1.2431361](https://doi.org/10.1063/1.2431361)]

## I. INTRODUCTION

Surfaces and interfaces of aqueous salt solutions are ubiquitous in nature and play important roles in phenomena as diverse as transport of ions across cell membranes, signal transmission through neural networks, release of reactive halogens into the atmosphere, and thundercloud electrification.<sup>1-4</sup> Insight into the structure of such interfaces has, therefore, wide-ranging implications for basic science. Moreover, progress in this area can potentially improve a wide variety of industrial processes which involve salt solutions. It is not surprising, therefore, that salt solutions and their interfaces enjoyed a significant scientific interest for more than a century.<sup>5</sup> Most thermodynamical properties of the surfaces of such solutions are well understood, with only a few controversial issues being still unsettled.<sup>6-8</sup> By con-

trast, experimental studies addressing the nanoscale structure of such surfaces are still very few, and their results are highly contradictory.<sup>9-11</sup> Among the dozens of theoretical models, suggested since the beginning of the last century,<sup>12</sup> some maintain that the near-surface region is completely devoid of ions, while others find significant ion adsorption at the surface phase. These contradictory results are discussed in the next section.

X-ray reflectivity (XR) is among the most powerful techniques for exploring the surface structure of liquids and solids with atomic resolution. The high x-ray fluxes and energy tunability, provided by third-generation synchrotron sources, were employed in this study to measure the reflectivity  $R(q_z)$  off the free surfaces of several concentrated salt solutions up to  $q_z=0.8$  Å<sup>-1</sup>, where  $q_z$  is the wave vector transfer normal to the liquid surface. A range of salt solutions were studied. To trace the dependence on the anion and cation, and their size differences, we have chosen to study the alkali halides RbBr,

<sup>a)</sup>Deceased.

<sup>b)</sup>Electronic mail: [deutsch@mail.biu.ac.il](mailto:deutsch@mail.biu.ac.il)

LiBr, CsCl, and RbCl. To explore the influence of the cation valence, a divalent salt ( $\text{SrCl}_2$ ) was studied as well. The concentrations investigated range from 2.7 to 13 m. Wavelengths tuned to the vicinity of the Br  $K$  edge were employed to detect possible specific Br ion adsorption to the surface in RbBr. The results are critically compared with available non-structural experimental results and used to test the validity of theoretical and simulational structural results published recently.<sup>12</sup>

## II. THEORETICAL AND EXPERIMENTAL BACKGROUND

It is now a well-established empirical fact that the surface tension of *concentrated* salt solutions,  $\gamma(c)$ , increases linearly with the concentration  $c$  of the anion, with a slope depending almost exclusively on the nature of the anion.<sup>13</sup> The higher-than-water surface tension of concentrated salt solutions implies an overall depletion of salt ions at the free surface.<sup>14</sup> By contrast, for *dilute* solutions of millimolar concentrations the opposite behavior is observed, with  $\gamma$  decreasing slightly with increasing  $c$ . This phenomenon, known as the Jones-Ray effect,<sup>6,15,16</sup> remains a mystery for the last 50 years and can neither be explained nor written off as an artifact.

The surface potential increment<sup>8,17</sup>  $\Delta\chi$  of salt solutions over that of pure water is positive for most of the classical salts (KI, KBr, KCl,  $\text{NaClO}_4$ , etc.). This implies an excess of anions over cations at the surface. Similar to  $d\gamma/dc$ ,  $d(\Delta\chi)/dc$  is also found to be almost independent of  $c$  and to be determined to a large extent by the anion, supporting the conclusion of an excess of anions over cations at the surface.

The above exemplifies that our understanding of the physics underlying the microscopic structure, properties, and behavior of electrolytes is still rudimentary, in spite of a century of research.<sup>18</sup> The classical model developed by Onsager and Samaras<sup>19</sup> to account for the interfacial behavior of very dilute salt solutions regards water as a continuous dielectric medium with a dielectric constant of ( $\epsilon \approx 80$ ) ("primitive model of water") and neglects the inter-ion interactions. To maintain the continuity of the electric potential across the water/vapor interface, an effective force is invoked, acting upon all charges located in the vicinity of the interface. This force, usually described as emanating from a fictitious image charge at the opposite side of the boundary, repels solute ions from the surface of the solution. The  $\gamma(c)$  dependence predicted by Onsager and Samaras is qualitatively incorrect for concentrated solutions and does not reproduce the observed Jones-Ray effect at millimolar concentrations. The surface potential in the Onsager-Samaras model is equal to that of pure water and is independent of the salt concentration, both of which contradict the measured behavior of  $\Delta\chi(c)$ . In spite of its obvious physical oversimplifications, the complex mathematical nature of the original Onsager-Samaras model strongly inhibited the introduction into the model of more physically realistic modifications. Nevertheless, several modifications of this model were suggested.<sup>2,3,8,20-25</sup> None of these takes into account the roughening of the surface by thermally excited capillary

waves<sup>26</sup> nor the intrinsic surface roughness due to the finite molecular size. As a result, nonphysical discontinuities in the surface density profiles are obtained.<sup>20,23,24</sup> The surface tension and the surface potential values predicted by some of the above-mentioned simplistic theories are in reasonable agreement with experiment,<sup>2,23,27,28</sup> but the ion distribution profiles determined in these studies are highly contradictory. It is not even clear, whether the ions are repelled from<sup>2,19,20,23-25,27,28</sup> or attracted to<sup>3,22</sup> the free surface.

In recent years several groups carried out detailed simulations of the surface structure of aqueous salt solutions.<sup>29-35</sup> Most simulations show a certain degree of ion specificity at the surface. However, it is usually claimed<sup>31</sup> that simulations employing a nonpolarizable force field show effective ion depletion at the surface, while those using large polarizable ions show an enrichment, due to the distortion of the hydration shell in the vicinity of the interface. This distortion results in a significant imbalance in the electric field of the water molecules' dipoles, which in turn polarizes the ion. For sufficiently large and polarizable ions this compensates for the loss of ion-water electrostatic interactions at the surface and stabilizes the ion at the surface. The great advantage of the computer simulations is that they deal with the microscopic structure of the interface so that the surface density profiles can be readily calculated<sup>12</sup> and can be compared with the experimental results, as we do below.

Several experimental studies addressing the molecular-scale structure of the aqueous salt solutions' interfaces have also been published. These studies employed x-ray<sup>36</sup> and extreme ultraviolet<sup>37</sup> photoemission spectroscopies, vibrational sum-frequency generation (VSFG),<sup>9,10,32,38,39</sup> second harmonic generation (SHG),<sup>15,16,40,41</sup> and ellipsometry.<sup>11</sup> The results obtained in these studies are in some cases contradictory. While ellipsometry finds an ion-depleted surface layer,<sup>11</sup> the SHG results are analyzed in terms of Langmuir adsorption isotherms,<sup>15,16,40,41</sup> yielding an enhanced anion concentration at the free surface. The VSFG studies show a similar dichotomy. Raymond and Richmond report a reduction in the ion concentration at the surface relative to that in the bulk,<sup>9</sup> while Liu *et al.*<sup>10</sup> report an enhancement of the anion concentration at the surface. Bulk ion attraction to, or repulsion from, charged liquid surfaces<sup>42</sup> and liquid-liquid interfaces<sup>43</sup> have also been studied recently with techniques similar to those employed here.

In the following, we describe our experimental techniques, discuss and analyze our measured XR data, and compare the electron density profiles derived from our measurements with those predicted by recent computer simulation studies.<sup>29-32</sup>

## III. EXPERIMENT

The XR method used in this study is by now a well-established technique, where one measures the fraction  $R$  of the intensity of the incident beam that is reflected by the surface as a function of the incidence angle  $\alpha$  with respect to the surface. The reflectivity curve,  $R(\alpha)$ , can then be analyzed to yield the surface-normal density profile of the liquid surface. The details of the method are well described in nu-

merous publications<sup>44</sup> and will not be repeated here. In the following we will discuss only the technical issues relevant to the present measurements.

The salts and concentrations employed in this study were chosen to satisfy several criteria, some of them conflicting. First, the differences between XR curves of an ion-depleted surface and a nondepleted surface are very small. Thus, to maximize the XR contrast, high concentrations and high electron density atoms had to be employed. This consideration requires using high-solubility salts of high- $Z$  atoms. Second, the  $K$  or  $L$  edges of the ions had to be within the tunable energy range of the synchrotron sources used to allow carrying out resonant XR measurements. This implied third-row atoms for the  $K$  edges and sixth-row atoms for the  $L$  edges. Third, beam damage to the solution and the surface had to be avoided. Such damage is manifested in a variation of the measured XR with beam exposure time. This was indeed found, for example, for all of the few iodides that we studied and which are, therefore, not discussed here. Visual inspection of the beam-exposed iodide solutions also revealed a pronounced and progressive browning of the solution with exposure time. Finally, practical considerations had to be also taken into account, such as the availability of high-purity compounds, high-enough melting temperature to allow for a good bakeout (see below), etc.

## A. Sample preparation

LiBr (99.995+ %) and RbCl (99.99%) were purchased from Aldrich. SrCl<sub>2</sub> (99.9965%), RbBr (99.8%), and CsCl (99.999+ %) were obtained from Alfa-Aesar. All salts were baked for >8 h at temperatures >350 °C. All solutions were prepared with Millipore ultra-high-purity water ( $R = 18.2 \text{ M}\Omega \cdot \text{cm}$ ). All parts of the experimental apparatus coming into contact with the salts or the salt solution were cleaned with piranha solution. The samples were prepared by weight, the molality being determined by means of an electronic balance. The corresponding molar concentrations were determined from the published aqueous solution density tables.<sup>45</sup> Since the molarity/molality ratio is almost constant in the relevant range of concentrations and since the ion-specific effects are not very large, linear extrapolations were done for compounds and concentrations not listed in the tables. Teflon coated magnetic stirrers were used to mix each solution at room temperature for at least 30 min, in a tightly capped volumetric glass flask.

The surface tensions of all the solutions were measured by the Wilhelmy plate method<sup>46</sup> to check for the presence of any organic impurities. The sensitivity of our surface tension measurements for detection of possible organics adsorbed on the surface can be estimated from the well known equation of state of the two-dimensional ideal gas.<sup>46</sup> Our absolute surface tension values are stable to within about  $\pm 0.6 \text{ mN/m}$  and agree with the published values to within less than  $\Delta\gamma \approx 2 \text{ mN/m}$ .<sup>13</sup> Assuming that the entire  $\Delta\gamma$  stems from surface impurities of concentration  $\Gamma$ , then  $\Gamma = \Delta\gamma / (k_B T) \approx 5 \times 10^{-3} \text{ molecules}/\text{\AA}^2$ , where  $k_B$  is the Boltzmann constant. The surface tensions obtained for the samples before the bakeout process fell below the experimental values by as

much as 15 mN/m. Furthermore, they did not show a linear dependence on concentration at high concentrations and were changing significantly with time. Since none of our samples exhibited these effects after the bakeout, we conclude that non-negligible amounts of organics are present in commercial ultrapure salts. This, in turn, raises concerns about the accuracy of results obtained in several recent surface studies of aqueous salt solutions,<sup>9,15,16,36,37,40,41</sup> where the salts were reported to be used as received. Note, however, that some of the techniques used in these studies may be significantly less sensitive to organic impurities at the surface than XR and surface tension measurements. For example, in very fast experiments, like studies performed on a microjet surface,<sup>37</sup> contamination of the newly formed surface may be very low due to the relatively slow surface adsorption kinetics of the organic contaminants.<sup>8</sup>

## B. Experimental setup

### 1. Spectrometer and sample cell

XR measurements were carried out both at the NSLS, Brookhaven National Laboratory, and the APS, Argonne National Laboratory. At the NSLS the Harvard/BNL liquid surface diffractometer at beamline X22B (Ref. 47) was used, at a wavelength  $\lambda \approx 1.54 \text{ \AA}$ . The liquid surface spectrometer at the CMC-CAT beamline ID-9C (Ref. 48) at the APS was used for the anomalous reflectivity measurement at wavelengths straddling the Br  $K$  edge at  $\lambda = 0.92018 \text{ \AA}$ . An aluminum sample cell with Kapton x-ray windows was employed. The cell was hermetically sealed with an ambient atmosphere inside immediately after loading the sample. The samples consisted of  $\sim 0.7 \text{ ml}$  of solution, placed onto a rectangular  $35 \times 70 \times 3 \text{ mm}^3$  fused quartz wafer, covering it to a height of a few tenths of a millimeter. All the XR measurements were carried out at ambient temperature. The samples studied were stable with time, and the results obtained for a single sample were reproducible for at least 24 h. No observable beam damage effects could be found, even though at high angles, where the reflectivity is low, the full power of the incident beam, without absorbers, is allowed to impinge on the surface.

### 2. Measurement method

Since the reflectivity spans more than nine orders of magnitude, as shown in Fig. 1, intense beams must be employed to achieve acceptable statistics, reasonable counting times, and good signal/noise ratios. At low incidence angles, where the reflectivity is high, absorbers and small incidence slits (reducing the beam size) are employed to avoid saturating the detector. As the incidence angle increases, and the reflectivity decreases, progressively larger slits are used and more of the absorbers are removed, to increase the reflected flux.

This procedure allows achieving both good statistics and short measuring times. However, this is achieved at the cost of having to ensure that the opening of the slits and the removal of the absorbers do not introduce artifacts in the measured reflectivity curve. The slit opening is accounted for by the incident beam monitor. The rest is done by measuring

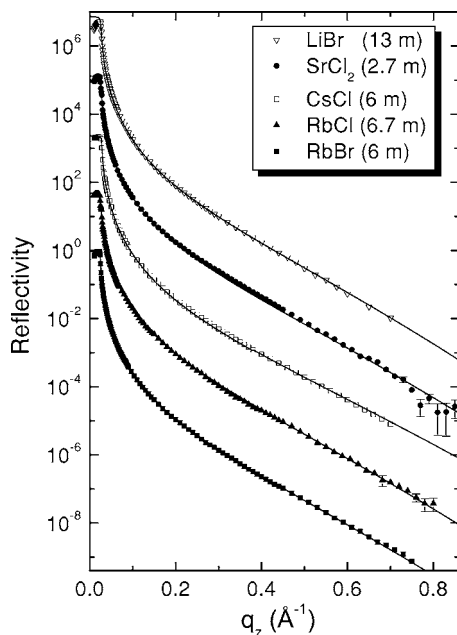


FIG. 1. The XR curves (symbols) for the salt solutions listed in Table I, with their fits, assuming an unstructured interface (lines). Curves are shifted vertically by factors of 50 for clarity.

the reflectivity at each crossover point with both the old and the new settings. The ratios of these values are used to scale the pieces of the reflectivity curve measured with the two settings. Note, however, that an increase in the incident beam slit size increases the x-ray footprint on the sample, so that the reflectivity is sampled over a larger surface area. Therefore, even with a perfectly aligned spectrometer, tiny inhomogeneities, or finite curvature of the liquid surface, can still introduce small mismatches at the crossover and, mainly, beyond.

The crossovers obtained in the present study are all within the 1% typical counting statistics of the measured points (except perhaps for the CsCl data). While in several cases very small mismatches at crossovers were fixed by introducing a constant relative intensity shift, the remaining crossover- and footprint-change-related intensity variations in the reflectivity curves are expected to be roughly of the same magnitude as the statistical error bars shown in the plotted curves.

### C. X-ray reflectivity

The x-ray reflectivity  $R$  is measured as function of the surface-normal component of the wave vector transfer,  $q_z = (4\pi/\lambda)\sin\alpha$ , where  $\alpha$  is the grazing angle of incidence of the x-ray beam onto the surface, and  $\lambda$  is the wavelength of the radiation. The XR off the surface of a multicomponent liquid depends on the surface-normal electron density profile, averaged over the lateral directions,  $\rho(z)$ , which is given by<sup>44,49</sup>

$$\rho(z) = \sum_i n^i(z) [f_i + f'_i(\lambda) + if''_i(\lambda)], \quad (1)$$

where  $f_i$ ,  $f'_i(\lambda)$ , and  $f''_i(\lambda)$  are the scattering factor and its real and imaginary dispersion corrections for the  $i$ th species.  $n^i(z)$

is the number density of the  $i$ th species along the surface-normal direction  $z$ . The summation is carried out over all species present in the sample. For our range of  $q_z$ , the wave vector dependence of the scattering factor can be neglected, and  $f_i \approx Z_i$ , where  $Z_i$  is the atomic number of the  $i$ th species. Note that  $f'_i$  is negligible for x-ray energies sufficiently far from a ionization thresholds. The dispersion corrections used in the present study were calculated *ab initio*<sup>50</sup> using the IFEFFIT software.<sup>51</sup> The sharp absorption edges are broadened by the finite lifetimes of the atomic levels. The lifetime widths were taken from the EADL project tables.<sup>52</sup>

It is important to note that the term “electron density profile,” widely used for  $\rho(z)$  as defined in Eq. (1), is somewhat inaccurate. The term “scattering power density profile” describes  $\rho(z)$  more accurately. The proper *electron density profile* is  $\sum_i n_i(z)Z_i$ . This quantity is well approximated by  $\rho(z)$  when three conditions are fulfilled: (a)  $q_z$  is small ( $f_i \approx Z_i$ ), (b) the x-rays’ wavelength is far from an absorption edge ( $f'_i \ll f_i$ ), and (c) absorption is negligible ( $f''_i \ll f_i$ ). These conditions hold, in our case, over the full  $q_z$  range measured when the x rays used have wavelengths not too close to the absorption edges of the ions. At the edge, however, the scattering power density profile is not identical with the electron density profile. To conform to common practice, we will keep using the term electron density profile for  $\rho(z)$ , trusting the reader to keep the caveat above in mind.

An experimental determination of the dispersion corrections in the vicinity of the Br  $K$  edge was attempted as well. For this purpose, a solid KBr sample was placed in the beam, and the transmission was measured as function of the incident beam’s energy over a range including the Br  $K$  edge. The attenuation length measured this way is proportional to the imaginary component of the dispersion correction  $f''(\text{Br})$ .<sup>44</sup> The real component  $f'(\text{Br})$  is readily calculated from the experimental  $f''(\text{Br})$  by applying the Kramers-Kronig (KK) transform.<sup>44</sup> The CHOOCH program<sup>53</sup> was used to perform the KK transform numerically. The deviations of the theoretical Dirac-Hartree-Fock  $[Z + f'(\text{Br})]$  values from the ones obtained by KK transformation of the experimental data are below 2%. We have neglected  $f''$  in all calculations (unless otherwise specified, see below) after making sure that its influence on the results is negligibly small.

### IV. RESULTS

The measured reflectivity curves  $R(q_z)$  are shown in Fig. 1 for four monovalent (alkali halide) and one divalent salt solutions. All XR curves exhibit a monotonic decay with  $q_z$ . Over the  $q_z$  range measured, the reflectivity decays by almost ten orders of magnitude, as discussed above. The decay is faster than  $q_z^{-4}$  due to the roughening of the liquid surface by thermally excited capillary waves, and by the intrinsic roughness<sup>54</sup>  $\sigma_0$ , arising mostly from the finite size of the atoms and the zero-point motion. The capillary waves scatter the radiation off specularly. However, photons scattered at small off-specular angles are still counted along with the reflected beam due to the finite acceptance angle of the detector. An integration of the off-specular scattering cross sec-

TABLE I. Sample details and fit results.  $c$  and  $M$  are the molalities and molarities of the solutions,  $E$  is the x-ray energy employed in the  $R(q_z)$  measurements, and  $\sigma_0$  and  $\sigma_e$  are the intrinsic and effective surface roughnesses obtained from the fits shown in Fig. 1, as discussed in the text.

	LiBr	SrCl <sub>2</sub>	CsCl	RbCl	RbBr
$c$	13.0	2.7	6.0	6.7	6.0
$M$	9.5	2.5	4.7	5.4	4.9
$E$ (keV)	8.14	13.474	13.474	15.400	13.274
$\sigma_0$ (Å)	1.9	1.5	1.3	1.6	1.6
$\sigma_e$ (Å)	3.0	2.9	2.7	2.9	2.9

tion over the resolution window of the detector was therefore carried out to account accurately for this effect.<sup>55</sup>

For a given  $\rho(z)$  profile, the reflectivity can be written as<sup>44,46,49</sup>

$$R(q_z) = R_\sigma(q_z) |\Phi(q_z)|^2 \exp(-\sigma_0^2 q_z^2), \quad (2)$$

where  $R_\sigma(q_z)$  is the reflectivity from an ideally flat and abrupt interface [the reflectivity of which is the Fresnel reflectivity,  $R_F$  (Ref. 44)], roughened only by the thermally induced capillary waves, of an effective amplitude  $\sigma_T$ , and  $\exp(-\sigma_0^2 q_z^2)$  accounts for the temperature independent intrinsic roughness. Denoting the effective electron density of the bulk by  $\rho_b$ , the structure factor  $\Phi(q_z)$  of the surface can be written as

$$\Phi(q_z) = \rho_b^{-1} \int_{-\infty}^{\infty} [d\rho(z)/dz] \exp(iq_z z) dz. \quad (3)$$

We have analyzed the XR curves in several steps. First, we assumed the interface to be unstructured:  $\Phi(q_z)=1$ . The  $R_\sigma(q_z)$  term in Eq. (2) can be evaluated accurately by integrating numerically the scattering cross section of the capillary waves using the known surface tension and the solid angle of acceptance of the detector.<sup>46</sup> The expression in Eq. (2) can now be fitted to the measured  $R(q_z)$  with the intrinsic interfacial width  $\sigma_0$  being the only adjustable parameter. These fits are shown as lines in Fig. 1 and exhibit an excellent agreement with the measured  $R(q_z)$ . The  $\sigma_0$  values obtained from the fits are listed in Table I. A different analysis

consisted of a phenomenological fit, assuming only one,  $q_z$ -independent, *effective* roughness parameter,  $\sigma_e$ , which includes the effect of both the intrinsic and the capillary-wave-induced roughnesses. This fit was done by setting  $\sigma_T=0$  and using  $\sigma_0$  as the only adjustable parameter in Eq. (2). Its fitted value, listed also in Table I, was taken as  $\sigma_e$ .

Almost identical  $\sigma_0$  values were obtained for all salts. These values can be understood by a simple geometrical model of spheres packed on a plane. The surface-normal profile of such a layer is  $\rho(z')/\rho_b = z'(2-z')$ , where  $0 \leq z' = z/a \leq 1$  is the reduced depth into the layer, and  $a$  is the radius of the spheres. The corresponding roughness of the top of this layer due to the spherical shape of the spheres can be calculated numerically as  $\sigma_0 \approx 0.3a$ . The bare ionic radii of the ions addressed in this study range from  $r_{\text{Li}^+} = 0.68$  Å to  $r_{\text{Br}^-} = 1.96$  Å, yielding intrinsic roughness values below 0.6 Å.<sup>45</sup> The hydrated radii of the same ions range up to 4.12 Å (for  $\text{Sr}^{+2}$ ).<sup>56</sup> When using the radii of the hydrated, rather than of the bare ions, the contributions to the  $\sigma_0$  range up to 1.25 Å. Considering that  $\sigma_0$  may also include contributions from thermally induced roughness on scales below the capillary waves cut off by the ionic (or hydrated-ionic) size, the agreement of these values with the fitted  $\sigma_0$  values in Table I is very reasonable.<sup>47,57</sup> This may indicate that the hydration shell of the ions is only slightly modified in the vicinity of the free interface. Note, however, that the concept of an ionic hydration shell may not be always well defined in very concentrated salt solutions. Among our samples there is just one such case, LiBr, where the ratio of salt ions to water molecules in the bulk is 26:55. With so few water molecules per ion the classical “dressed ion” picture is clearly invalid. Taking all these into account, the good correspondence between the experimental and the theoretical  $\sigma_0$  values is rather remarkable.

To detect more accurately possible deviations of the measured  $R(q_z)$  from that of a monotonic, unstructured density profile broadened by capillary waves, we normalize both the measured  $R(q_z)$ , and its fits in Fig. 1, by the Fresnel reflectivity  $R_F(q_z)$  off a perfectly smooth and abrupt surface. These curves are shown in Fig. 2(a). This normalization reduces the average variation of  $R/R_F$  to three orders of mag-

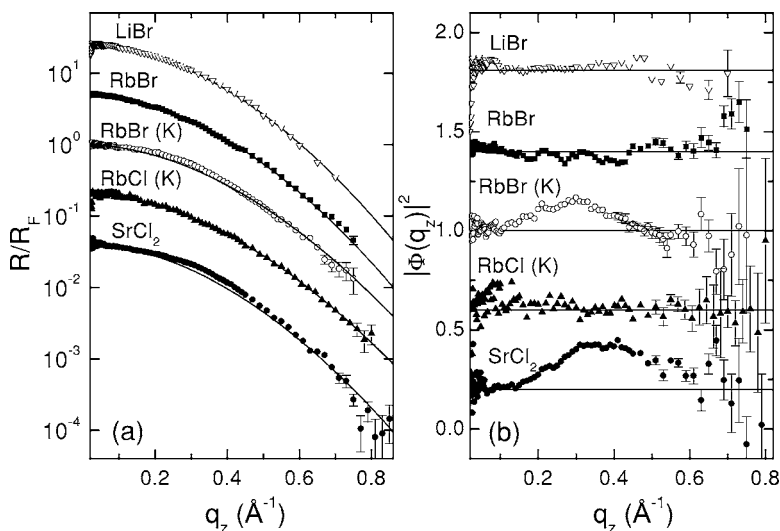


FIG. 2. (a) The Fresnel-normalized measured (symbols) and fitted (lines) XR curves for the samples listed in Table I. The fit assumes an unstructured interface, with a monotonic density profile. The RbBr and the RbCl curves marked by K were measured at the K edges of Br (13.474 keV) and Rb (15.230 keV), respectively. Curves are shifted vertically by factors of 5 each for clarity. (b) The measured XR curves in (a) divided by their theoretical fits. Only RbBr(K) and SrCl<sub>2</sub> deviate from unity (solid horizontal lines). For discussion see text. Curves are shifted vertically for clarity.

nitude instead of the nine to ten orders of the variation of  $R$  in Fig. 1. However, even on this scale the agreement of the theoretical curves with experiment is still good, and only  $\text{SrCl}_2$  shows some deviations. We next divide the  $R/R_F$  curves by the theoretical fits. The resultant curves, shown in Fig. 2(b), are the structure factors squared,  $|\Phi(q_z)|^2$ , of the corresponding surfaces. Any deviations of these from unity imply a structured interface, the surface-normal density profile of which deviates from a monotonic, roughness-broadened step function. As can be observed in Fig. 2(b), no such deviations occur for  $\text{LiBr}$ ,  $\text{RbBr}$ , and  $\text{RbCl}$ , implying that these solutions have simple density profiles, rising from zero at the vapor to that of the bulk smoothly and monotonically. Only the resonant  $\text{RbBr}$  and the (nonresonant)  $\text{SrCl}_2$  show deviations from unity, implying possible structure. The reflectivity of  $\text{SrCl}_2$ , which shows the largest deviation, was measured both at the APS and the NSLS to reduce the possibility of artifacts. The results obtained at both sources show the same peak, centered at  $q_z \approx 0.4 \text{ \AA}^{-1}$ , supporting the reproducibility of the results shown in Fig. 2(b).

## V. DISCUSSION

For all but two of the solutions studied here, a monotonic density profile was found, of width commensurate with the surface tension and intrinsic roughness. Since nothing more can be said about the density profile of these, we will focus in this section on the two samples which show evidence for surface segregation of ions. This segregation is manifested in the deviation of the experimentally derived  $|\Phi(q_z)|^2$  from unity. We first compare our results with recent computer simulations and then derive the density profiles from  $|\Phi(q_z)|^2$  by box-model fits.

### A. Comparison with computer simulations

The simulations of Jungwirth and Tobias<sup>29–32</sup> (JT) have recently attracted significant interest,<sup>12</sup> as they provide an explanation for several geophysical phenomena.<sup>4</sup> These simulations show that small nonpolarizable ions, e.g.,  $\text{Na}^+$  and  $\text{F}^-$ , are depleted from the surface. However, for large polarizable anions such as  $\text{I}^-$  and  $\text{Br}^-$ , a significant enhancement of the surface concentration occurs. Moreover, for salts such as  $\text{NaI}$ , the increased surface concentration of  $\text{I}^-$  induces a positively charged counterion layer of  $\text{Na}^+$  next to the surface. As discussed above, our samples and concentrations were chosen to satisfy several criteria to allow high accuracy XR measurements. Unfortunately, the salts and concentrations chosen were not addressed by the simulations published in the literature, and thus a straightforward comparison with the available simulations is not possible. However, as described in Sec. II, the thermodynamics of the surface (i.e., the surface tension and the surface potential) are mainly determined by the nature of the anion. We therefore assume that the results of the simulations obtained for a  $\text{NaBr}$  solution<sup>29</sup> are valid also for the  $\text{RbBr}$  solutions which we measured, since both have the same  $\text{Br}^-$  anion. Admittedly, the conclusions derived below on the agreement, or otherwise, of the simulations with the measurements presented here rest upon the validity of this assumption.

Computer simulations never reach the thermodynamical limit due to storage and time constraints. For example, the study of JT consists of a total of  $\sim 1000$  molecules. The reduced lateral dimensions of the simulated system, as compared to a real sample, result in the exclusion from the surface of capillary waves of wavelengths longer than the dimension of the simulated system.<sup>58</sup> This seems to be the reason for the anomalously low interfacial width (about  $1 \text{ \AA}$ ) obtained by JT. The reflectivities derived from density profiles with such unphysically low roughnesses are much higher than the corresponding experimental data over almost all of the measured  $q_z$  range. For example, at  $q_z = 0.8 \text{ \AA}^{-1}$ , the reflectivity from such a low-roughness interface would be at least 50-fold higher than that observed experimentally. To account properly for the full spectrum of capillary waves existing in the experimentally measured sample, we have multiplied the reflectivity curves obtained from the simulated density profiles by an additional Debye-Waller factor, the magnitude of which was optimized to match the measured data.

The surface-normal  $\text{Na}^+$  density profile (for  $\text{NaBr}$ ), shown by JT,<sup>29,31</sup> extends to a depth of  $\sim 16 \text{ \AA}$  below the surface. However, at a depth of  $9\text{--}10 \text{ \AA}$  the main near-surface density enhancement peak of the  $\text{Na}^+$  layer is already down to almost the density level of the bulk. We therefore cut off the  $\text{Na}^+$  density profile at around  $9\text{--}10 \text{ \AA}$  below the surface and use the bulk density value at larger depths. Other ways to extend the density profile to depths larger than those provided in the simulations were also attempted. These were the following: (1) multiply the density profile at depths smaller than  $16 \text{ \AA}$  by 1.25 to make the  $\text{Na}^+$  density at a depth of  $16 \text{ \AA}$  equal to that of the bulk, or (2) use a monotonic, smooth error function to interpolate between the  $\text{Na}^+$  density at  $16 \text{ \AA}$  and that of the bulk. The two alternative approaches did not alter the corresponding calculated reflectivities significantly, as compared to that obtained from the procedure used by us.

Figures 3(a) and 3(b) show  $|\Phi(q_z)|^2$  (dash-dot lines) calculated using Eq. (3) from the simulated density profiles of JT. Note, however, that those were calculated for a  $1.2M$  solution, lower than ours. Thus, the JT density profile of each ion was multiplied by a factor that raised its bulk concentration from the lower value of the simulated solution to the higher value of the solution studied here experimentally. This scaling is equivalent to the reasonable assumption that the surface/bulk concentration ratio of each ion is independent of the concentration at these high molarities. The  $|\Phi(q_z)|^2$  curves obtained from the scaled density profiles are shown in dashed lines in Fig. 3.

Finally, the simulations performed for  $\text{NaCl}$  (Ref. 32) were used to calculate the electron density profile for  $\text{SrCl}_2$ , shown in Fig. 3(c). Since  $\text{NaCl}$  and  $\text{SrCl}_2$  have different valence cations, we show (dashed line) only the  $|\Phi(q_z)|^2$  calculated for the profile which was scaled to the bulk concentration of our experiment:  $\text{Sr}^+$  ( $2.7m$ ),  $\text{Cl}^-$  ( $5.4m$ ), and  $\text{H}_2\text{O}$  ( $55.5m$ ).

Overall, the results derived from the simulations, shown in Fig. 3, do not show a good agreement with the measured  $|\Phi(q_z)|^2$ . While for the  $\text{RbBr}$  sample measured at the  $K$  edge

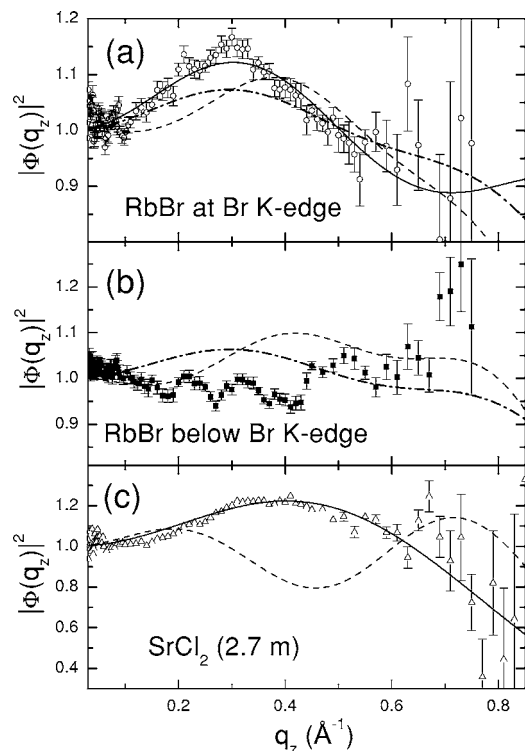


FIG. 3. The measured (symbols)  $|\Phi(q_z)|^2$  for a  $6m$  RbBr solution (a) and (b) 200 eV below the Br  $K$  edge. (c) Same for a  $2.7m$  SrCl<sub>2</sub> solution. The dashed-dot lines were calculated from the simulations of Jungwirth and Tobias (Ref. 29) for a  $1.2M$  solution. The dashed lines were calculated from the same simulations with bulk ion concentrations scaled to those of our measurements, as described in the text. The solid lines are fits by a simple single-slab box model, discussed in the text. The two small-period oscillations observed at  $0.2 \leq q_z \leq 0.4$  in the off-resonant data (b) are only slightly larger than the statistical error bars and are most probably an artifact due to the necessary slit changes performed during the XR scan, which spans nine orders of magnitude in intensity, as described in Sec. III.

[Fig. 3(a)] the dashed curve seems to reproduce the observed oscillation albeit somewhat shifted, the same sample measured below the edge [Fig. 3(b)] is far from the calculated dashed line. The situation for SrCl<sub>2</sub> [Fig. 3(c)] is even worse:  $|\Phi(q_z)|^2$  calculated from the simulations exhibits a dip centered on  $q_z \approx 0.45 \text{ \AA}^{-1}$ , where the measurements show a

peak. The twofold smaller oscillation period exhibited by the dashed line cannot be improved by any choice of the roughness parameter.

It is possible that the dichotomy between our results and the simulations stems from a qualitative change that occurs in the ionic density profiles at a concentration intermediate between the high concentration of our experiments and the lower concentration of the simulations. This would invalidate the simple scaling that we employed. Indeed, at the very high ionic strengths encountered in our studies, the surface concentration of water molecules is low and may result in a reduced shielding of the ion-ion interactions. This, in turn, may result in a nonlinear behavior of the profile as a function of the ion density. If indeed this is the case, the computer simulations manifest a reentrant evolution of the density profile with concentration, where the oscillatory surface profile exists for intermediate concentrations, but disappears both at the low concentration limit, where the classical treatment is applicable,<sup>19</sup> and at the high concentration limit, studied here. Unfortunately, such an effect would be almost impossible to detect experimentally, since even at the high concentrations employed here, the structure factors barely differ from unity. Lower concentrations will likely reduce the deviation of the structure factor from unity below the detection limit of the XR measurements. We hope that future simulations will address the higher concentrations studied here so that a more straightforward simulation-experiment comparison, not requiring any scaling, could be carried out.

## B. Box-model fits

The simplest model<sup>46</sup> to account for the  $|\Phi(q_z)|^2$  in Figs. 3(a) and 3(c) is a  $\rho(z)$  consisting of a single surface layer of constant electron density  $\rho_s$  different from that of the bulk  $\rho_b$ . The thickness of the layer is denoted by  $d$ , and all interfaces are assumed to be broadened by the intrinsic roughness  $\sigma_0$ . This single-slab model includes, therefore, three adjustable parameters:  $d$ ,  $\rho_s$ , and  $\sigma_0$ . In principle,  $\rho_s$  is a complex number [see Eq. (1)]. However, the imaginary component is much smaller than the real one and can be neglected anywhere except near an absorption edge.<sup>44</sup> In Fig. 4(a) we plot

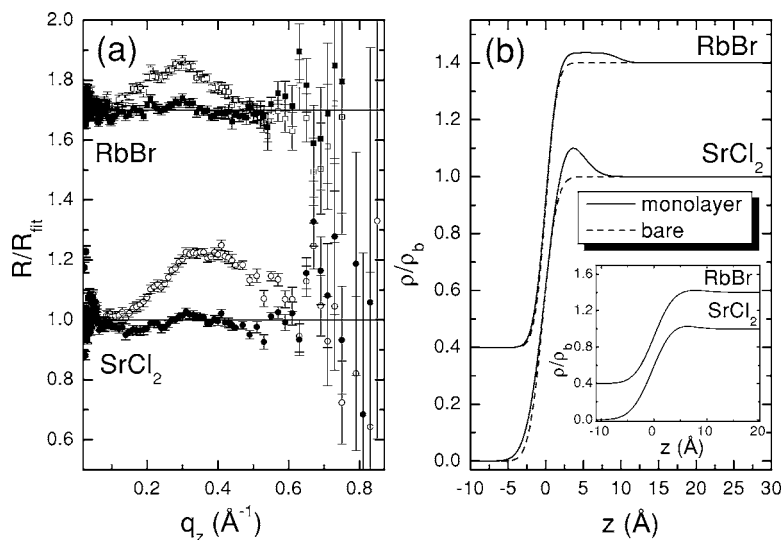


FIG. 4. (a) The measured reflectivity normalized to the fitted one, when the fit assumes a structured (solid symbols) and unstructured (open symbols) electron density profile, for a  $6m$  RbBr solution at the Br  $K$  edge and for a  $2.7m$  SrCl<sub>2</sub> solution. (b) The structured (solid line) and unstructured (dashed line) density profiles, unmodified by capillary waves (i.e., at  $T=0$ ) obtained in the fits and used to calculate  $R_{\text{fit}}$  used in (a). The RbBr curves are shifted up by (a) 0.7 and (b) 0.4 for clarity. Inset: capillary-wave-modified (i.e., room-temperature) density profiles of the structured RbBr and SrCl<sub>2</sub> solutions.

the reflectivity  $R$  of the 6*m* RbBr solution, measured at the Br  $K$  edge, and of the 2.7*m* SrCl<sub>2</sub> solution. For each salt,  $R$  is shown normalized by the fitted model,  $R_{\text{fit}}$ , calculated assuming an unstructured, monotonic density profile (open symbols) or a surface-enhanced, structured, profile (solid symbols). These profiles are shown in Fig. 4(b). The deviations from unity in Fig. 4(a) for the normalization by the  $R_{\text{fit}}$  of the unstructured profile do not exceed 20%, for both solutions. This is rather small, considering that the reflectivity curves (Fig. 1) extends over almost ten-orders of magnitude. On the other hand, the good quality of the fits when using the surface-enhanced density profiles is demonstrated by the fact that the ratio  $R/R_{\text{fit}}$  (solid symbols) in Fig. 4(a) is equal to unity, within the statistical scatter of the data, for all  $q_z$ .

The profiles shown in Fig. 4(b) include only the nonthermal roughness term  $\exp(-\sigma_0^2 q_z^2)$ . They correspond, therefore, to a temperature of  $T=0$  K. At finite temperatures the thermally excited capillary waves introduce further roughening, included in the  $R_\sigma$  term in Eq. (2). This roughening invariably smears out local deviations from unity in  $\rho(z)/\rho_b$ . Indeed, the physically relevant room-temperature profiles, shown in the inset to Fig. 4(b), exhibit much smaller density enhancements at the surface than their  $T=0$  K counterparts.

The  $|\Phi(q_z)|^2$  curves in Figs. 3(a) and 3(c) show only a single peak of a rather modest height above unity. These characteristics lead to a non-negligible interdependence in the fitted values of the three free parameters used to define the single-slab density model. Equal-quality fits to that shown in Fig. 3 can be obtained for other values of  $d \leq 15$  Å for RbBr and  $\leq 10$  Å for SrCl<sub>2</sub>. The  $\sigma_0$  and the  $\rho_s$  values obtained from the fits for each choice of the interfacial thickness  $d$  are shown in Fig. 5, where the abscissa is extended down to  $d$  values which are unphysically low, to allow following trends in the results. The  $R/R_{\text{fit}}$  curves obtained for  $d=0.1$  Å and  $d=1$  Å (and the corresponding  $\sigma_0$  and  $\rho_s$  of each  $d$ ) for RbBr are indistinguishable from that shown in solid symbols in Fig. 4(a), on the scale of the figure.

Note that in Fig. 5, for very small  $d$ ,  $\sigma_0$  becomes independent of the choice of  $d$ , and  $|\Phi(q_z)|^2$  depends mostly on the product  $\rho_s \times d$ . This general observation<sup>59</sup> is the reason for the linear behavior of  $\rho_s(d)$  in Fig. 5(b) at low  $d$  values for both salts. In the inset we show the surface density values obtained in the fits for  $d > 6$  Å on a magnified scale.

We now proceed to show that the  $\rho(z)$  enhancement observed for RbBr at the surface is consistent with a depletion of the surface of Br<sup>-</sup> ions. The reflectivity from the same RbBr sample was measured at three different energies: 13.274 keV (Figs. 2 and 3), 13.474 keV (Figs. 2–4), and 13.674 keV. Only the resonant reflectivity at the Br  $K$  edge (13.474 keV) exhibits significant deviations of the structure factor from unity. We conclude, therefore, that the surface enhancement in  $\rho(z)$  obtained in Fig. 4(b) for the resonant (13.474 keV) RbBr results from the strong energy dependence of  $f'(\text{Br})$ . The effective total *bulk* electron density of a 6*m* RbBr solution  $\pm 200$  eV away from the Br  $K$  edge is  $0.464 \text{ e}/\text{\AA}^3$ . At the edge, however,  $f'_{\text{Br}}$  exhibits a sharp minimum and the bulk electron density reduces to  $0.448 \text{ e}/\text{\AA}^3$ . Our measurements show that away from the edge  $|\Phi(q_z)|^2$

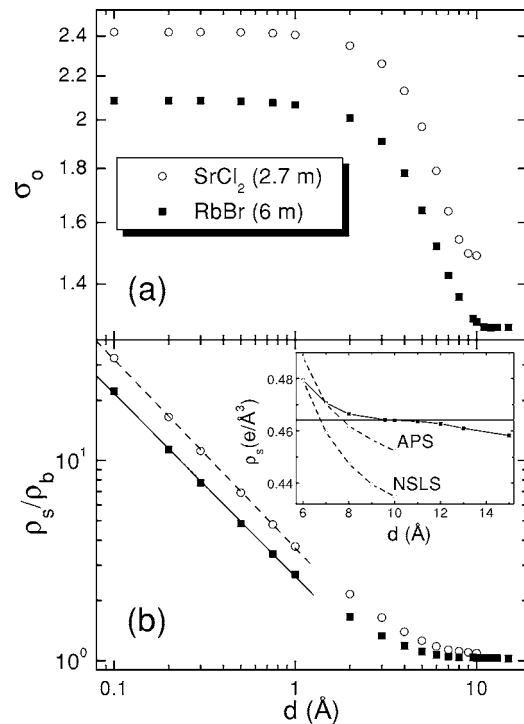


FIG. 5. The interdependence of the fit parameters of the single-slab model. (a) The  $d$  dependence of the intrinsic roughness. Note the constant value at small  $d$ . (b) Same for the surface layer density, normalized by that of the bulk. Note the linear dependence,  $\log(\rho_s/\rho_b) = 0.419 - 0.915 \log(d)$  for RbBr and  $\log(\rho_s/\rho_b) = 0.562 - 0.942 \log(d)$  for the SrCl<sub>2</sub>, at small  $d$ . Inset: unnormalized  $\rho_s$  values for the physically relevant range of  $d$ . Points above the horizontal solid line at  $\rho_s = 0.464 \text{ e}/\text{\AA}^3$  are unphysical as explained in the text. The same symbols are used for the corresponding quantities in the inset and in the main figure.

$= 1$ , so that  $\rho_s = \rho_b = 0.464 \text{ e}/\text{\AA}^3$ . If the surface concentration of Br<sup>-</sup> ion were that of the bulk, then  $\rho_s = \rho_b$  always holds, and therefore  $|\Phi(q_z)|^2 = 1$  would result at the  $K$  edge. If the Br<sup>-</sup> concentration at the surface is larger than in the bulk,  $\rho_s < \rho_b$  would be observed at the  $K$  edge. The only way to explain the apparent enhancement of  $\rho(z)$  at the surface,  $\rho_s > \rho_b$ , is to have a depletion of Br<sup>-</sup> ions at the surface, so that  $\rho_s$  stays  $0.464 \text{ e}/\text{\AA}^3$  at the  $K$  edge. This will appear as a surface enhancement in the *bulk normalized* profile,  $\rho(z)/\rho_b$ , shown in Fig. 4(b) (solid line).

The argument above also sets an upper limit of  $0.464 \text{ e}/\text{\AA}^3$  for the surface electron density  $\rho_s$  of RbBr. This value is shown as a horizontal solid line in the inset to Fig. 5(b). This, in turn, sets a lower limit on the physically acceptable value of the surface layer thickness  $d$ . We conclude, therefore, that the surface layer of the RbBr is Br<sup>-</sup> depleted, has a thickness  $d$  between 10 and 15 Å, and has an intrinsic roughness of about 1.3 Å.

A stringent test on this conclusion and its preceding arguments is a simultaneous fit of both RbBr reflectivities, the one measured at the  $K$  edge and the other away from the edge. The surface number densities of the components (Rb<sup>+</sup>, Br<sup>-</sup>, H<sub>2</sub>O) and the layer thickness  $d$  are used as fit parameters, equal for both the resonant and the nonresonant data sets. This entails the explicit introduction, in both surface and bulk phases, of both the imaginary,  $f'(\text{Br})$ , and the real,  $f''(\text{Br})$ , parts of the dispersion correction. The intrinsic

roughness is fitted independently for the resonant and the nonresonant data, yielding  $\sigma_0 = 1.3 \pm 0.1 \text{ \AA}$  and  $\sigma_0 = 1.5 \pm 0.1 \text{ \AA}$ , respectively. The number density of the  $\text{Br}^-$  ions at the surface converges to zero. The surface number density of  $\text{Rb}^+$  ions is obtained as  $(5.2 \pm 0.1) \times 10^{-3} \text{ \AA}^{-3}$ , which is about twice the bulk density of  $\text{Rb}^+$ . The repulsive Coulombic interaction between the  $\text{Rb}^+$  cations is likely screened by the water molecules, which are present at the surface in about the same concentration,  $2.8 \times 10^{-2} \text{ \AA}^{-3}$ , as in the bulk:  $2.7 \times 10^{-2} \text{ \AA}^{-3}$ . Earlier neutron studies<sup>60</sup> of the  $\text{RbBr}$  and  $\text{RbCl}$  bulk aqueous solutions set  $7 \pm 0.9$  as the *upper limit* on the number of water molecules in the first hydration shell of  $\text{Rb}^+$ , also at much higher water concentrations. Therefore, each of the  $\text{Rb}^+$  cations in our  $\text{Br}^-$  depletion layer has its own complete hydration shell. Further screening may be provided by the smearing out of the depletion layer at room temperature by the thermally induced capillary waves, as discussed above. The thickness of the  $T=0 \text{ K}$  surface layer can be tuned to any value between 7 and 11  $\text{\AA}$ , with very little influence on all the other parameters and on the quality of the fit. These results are very close to those shown in Fig. 5(b) (solid symbols), which were obtained by neglecting the imaginary part of the dispersion correction, indicating that  $f''$  is only of marginal significance here.

We speculate that a depletion of the anions at the surface, found above for  $\text{RbBr}$ , may also occur in  $\text{SrCl}_2$ , causing the observed increase in  $\rho(z)$ . This occurs since with an ionic radius of 1.81  $\text{\AA}$  for the  $\text{Cl}^-$  ion<sup>61</sup> and 17 electrons, its electron density is considerably lower than that of the  $\text{Sr}^{+2}$  ion, which has an ionic radius of 1.27  $\text{\AA}$ ,<sup>61</sup> and over twice the number of electrons. This inference, however, must be verified by resonant XR measurements at the Sr *K* edge. Moreover,  $\text{RbCl}$  and  $\text{CsCl}$  for which the cations also have high electron densities exhibit only monotonic unstructured profiles.

Finally, we wish to point out again that the deviations of the measured  $|\Phi(q_z)|^2$  of  $\text{RbBr}$  and  $\text{SrCl}_2$  from the  $|\Phi(q_z)|^2 = 1$  of an unstructured, monotonic, interface are very small. Moreover, the results derived in Figs. 4 and 5 were obtained employing a specific model, which, although simple, may not be unique.<sup>62</sup> Measurements with better statistics over an extended  $q_z$  range would enhance the confidence in the conclusion derived here. However, diffuse scattering by thermally excited surface capillary waves renders such measurements very challenging even at the most intense beamlines available at present at third-generation synchrotrons. Measurements on a larger number of different salts may also clarify why only  $\text{RbBr}$  and  $\text{SrCl}_2$ , among all electrolytes studied here, show nonmonotonic  $\rho(z)$  profiles.

## VI. CONCLUSION

XR measurements on several concentrated salt solutions reveal monotonic, unstructured  $\rho(z)$  profiles. Only two solutions, a 6*m*  $\text{RbBr}$  and a 2.7*m*  $\text{SrCl}_2$ , show deviations from these profiles. A model consisting of a single surface layer of a constant scattering power density higher than that of the bulk was shown to be consistent with the measured XR curves of these two solutions. A comparison of the XR

curves measured for  $\text{RbBr}$  on- and off-resonance helped to limit the correlations between the fitting parameters of the model and suggested a depletion of  $\text{Br}^-$  ions at the surface. Our results disagree with recent simulations, which predict strong alternate layering of different charge ions at the surface. Future computer simulations and theoretical studies are called for to explain the microscopic-level origin and behavior of the surface-normal electron density profiles found here for high-concentration solutions of mono- and divalent salts.

## ACKNOWLEDGMENTS

The authors thank Yuguang Cai (BNL) for assistance and discussions. BNL is supported by U.S. DOE Contract No. DE-AC02-98CH10886. CMC-CAT is supported by OBES, U.S. DOE, and by NSF, Division of Materials Research. The APS is supported by U.S. DOE Contract No. W-31-109-Eng-38. Support by the U.S.-Israel Binational Science Foundation, Jerusalem, is gratefully acknowledged.

- <sup>1</sup>F. E. Bloom, A. Lazerson, and L. Hofstadter, *Brain, Mind and Behavior* (Freeman, New-York, 1988).
- <sup>2</sup>V. S. Markin and A. G. Volkov, *J. Phys. Chem. B* **106**, 11810 (2002).
- <sup>3</sup>M. Boström, D. R. M. Williams, and B. W. Ninham, *Langmuir* **17**, 4475 (2001).
- <sup>4</sup>E. M. Knipping, M. J. Lakin, K. L. Foster, P. Jungwirth, D. J. Tobias, R. B. Gerber, D. Dabdub, and B. J. Finlayson-Pitts, *Science* **288**, 301 (2000); K. L. Foster, R. A. Plastringer, J. W. Bottenheim, P. B. Shepson, B. J. Finlayson-Pitts, and C. W. Spicer, *ibid.* **291**, 471 (2001); A. Laskin, D. J. Gaspar, W. Wang, S. W. Hunt, J. P. Cowin, S. D. Colson, and B. J. Finlayson-Pitts, *ibid.* **301**, 340 (2003); P. Jungwirth, V. Rosenfeld, and V. Buch, *Atmos. Res.* **76**, 190 (2005).
- <sup>5</sup>A. Gradenwitz, *Phys. Z.* **3**, 329 (1902); A. Heydweiler, *Ann. Phys.* **33**, 145 (1910).
- <sup>6</sup>G. Jones and W. A. Ray, *J. Am. Chem. Soc.* **59**, 187 (1937); **63**, 288 (1941).
- <sup>7</sup>I. Langmuir, *Science* **88**, 430 (1938); *J. Chem. Phys.* **6**, 873 (1938).
- <sup>8</sup>J. E. B. Randles, *Phys. Chem. Liq.* **7**, 107 (1977).
- <sup>9</sup>E. A. Raymond and G. L. Richmond, *J. Phys. Chem. B* **108**, 5051 (2004).
- <sup>10</sup>D. Liu, G. Ma, L. M. Levering, and H. C. Allen, *J. Phys. Chem. B* **108**, 2252 (2004).
- <sup>11</sup>D. Beaglehole, *J. Phys. Chem.* **93**, 2004 (1989).
- <sup>12</sup>B. C. Garrett, *Science* **303**, 1146 (2004).
- <sup>13</sup>A. A. Abramzon and R. D. Gaukhberg, *Russ. J. Appl. Chem.* **66**, 1139 (1993); **66**, 1315 (1993); **66**, 1473 (1993); R. Aveyard and S. M. Saleem, *J. Chem. Soc., Faraday Trans. 1* **72**, 1609 (1976); K. Johansson and J. C. Eriksson, *J. Colloid Interface Sci.* **49**, 469 (1974); P. K. Weissenborn and R. J. Pugh, *ibid.* **184**, 550 (1996).
- <sup>14</sup>Z. B. Li, Y. G. Li, and J. F. Lu, *Ind. Eng. Chem. Res.* **38**, 1133 (1999); Z. Li and B. C. Y. Lu, *Chem. Eng. Sci.* **56**, 2879 (2001).
- <sup>15</sup>P. B. Petersen, J. C. Johnson, K. P. Knutsen, and R. J. Saykally, *Chem. Phys. Lett.* **397**, 46 (2004).
- <sup>16</sup>P. B. Petersen, R. J. Saykally, M. Mucha, and P. Jungwirth, *J. Phys. Chem. B* **109**, 10915 (2005).
- <sup>17</sup>N. L. Jarvis and M. A. Scheiman, *J. Phys. Chem.* **72**, 74 (1968).
- <sup>18</sup>W. Kunz, P. Lo Nostro, and B. W. Ninham, *Curr. Opin. Colloid Interface Sci.* **9**, 1 (2004).
- <sup>19</sup>L. Onsager and N. N. T. Samaras, *J. Chem. Phys.* **2**, 528 (1934); C. Wagner, *Phys. Z.* **25**, 474 (1924).
- <sup>20</sup>M. Manciu and E. Ruckenstein, *Adv. Colloid Interface Sci.* **105**, 63 (2003).
- <sup>21</sup>K. A. Karraker and C. J. Radke, *Adv. Colloid Interface Sci.* **96**, 231 (2002).
- <sup>22</sup>M. Boström, W. Kunz, and B. W. Ninham, *Langmuir* **21**, 2619 (2005).
- <sup>23</sup>L. B. Bhuiyan, D. Bratko, and C. W. Outhwaite, *J. Phys. Chem.* **95**, 336 (1991).
- <sup>24</sup>M. A. Wilson, A. L. Nichols III, and L. R. Pratt, *J. Chem. Phys.* **78**, 5129 (1983).
- <sup>25</sup>F. P. Buff and F. H. Stillinger, Jr., *J. Chem. Phys.* **25**, 312 (1956).

- <sup>26</sup>The only exception is the very recent work by Boström *et al.* (Ref. 22), which, however, uses the incorrect water surface roughness obtained by JT (Ref. 29) from computer simulations.
- <sup>27</sup>E. Schmutzer, *Z. Phys. Chem. (Leipzig)* **204**, 131 (1955).
- <sup>28</sup>K. Schäfer, A. Perez-Masia, and H. Jüntgen, *Z. Elektrochem.* **59**, 425 (1955).
- <sup>29</sup>P. Jungwirth and D. J. Tobias, *J. Phys. Chem. B* **105**, 10468 (2001).
- <sup>30</sup>P. Jungwirth and D. J. Tobias, *J. Phys. Chem. B* **105**, 6361 (2002).
- <sup>31</sup>L. Vrbka, M. Mucha, B. Minofar, P. Jungwirth, E. C. Brown, and D. J. Tobias, *Curr. Opin. Colloid Interface Sci.* **9**, 67 (2004).
- <sup>32</sup>M. Mucha, T. Frigato, L. M. Levering, H. C. Allen, D. J. Tobias, L. X. Dang, and P. Jungwirth, *J. Phys. Chem. B* **109**, 7617 (2005).
- <sup>33</sup>L. X. Dang and T. M. Chang, *J. Phys. Chem. B* **106**, 235 (2002); G. Luo, S. Malkova, J. Yoon, D. G. Schultz, B. Lin, M. Meron, I. Benjamin, P. Vanysek, and M. L. Schlossman, *Science* **311**, 216 (2006).
- <sup>34</sup>S. J. Stuart and B. J. Berne, *J. Phys. Chem. A* **103**, 10300 (1999).
- <sup>35</sup>D. Bhatt, J. Newman, and C. J. Radke, *J. Phys. Chem. B* **108**, 9077 (2004).
- <sup>36</sup>S. Ghosal, J. C. Hemminger, H. Bluhm, B. S. Mun, E. L. D. Hebenstreit, G. Ketteler, D. F. Ogletree, F. G. Requejo, and M. Salmeron, *Science* **307**, 563 (2005).
- <sup>37</sup>R. Weber, B. Winter, P. M. Schmidt, W. Widdra, I. V. Hertel, M. Dittmar, and M. Faubel, *J. Phys. Chem. B* **108**, 4729 (2004).
- <sup>38</sup>S. Gopalakrishnan, P. Jungwirth, D. J. Tobias, and H. C. Allen, *J. Phys. Chem. B* **109**, 8861 (2005).
- <sup>39</sup>M. J. Shultz, S. Baldelli, C. Schnitzer, and D. Simonelli, *J. Phys. Chem. B* **106**, 5313 (2002).
- <sup>40</sup>P. B. Petersen and R. J. Saykally, *Chem. Phys. Lett.* **397**, 51 (2004).
- <sup>41</sup>P. B. Petersen and R. J. Saykally, *J. Phys. Chem. B* **109**, 7976 (2005).
- <sup>42</sup>W. Bu, D. Vaknin, and A. Travesset, *Langmuir* **22**, 5673 (2006).
- <sup>43</sup>G. Luo, S. Malkova, J. Yoon, D. G. Schultz, C. Lin, M. Meron, I. Benjamin, P. Vanysek, and M. L. Schlossman, *Science* **311**, 216 (2006).
- <sup>44</sup>J. Als-Nielsen and D. McMorrow, *Elements of Modern X-Ray Physics* (Wiley, New York, 2001); M. Deutsch and B. M. Ocko, *Encyclopedia of Applied Physics*, edited by G. L. Trigg (VCH, New York, 1998), Vol. 23, p. 479.
- <sup>45</sup>*Handbook of Chemistry and Physics*, 65th ed., edited by R. C. Weas (CRC, Boca Raton, FL, 1984).
- <sup>46</sup>E. Sloutskin, B. M. Ocko, L. Tamam, I. Kuzmenko, T. Gog, and M. Deutsch, *J. Am. Chem. Soc.* **127**, 7796 (2005).
- <sup>47</sup>A. Braslau, P. S. Pershan, G. Swislow, B. M. Ocko, and J. Als-Nielsen, *Phys. Rev. A* **38**, 2457 (1988); M. K. Sanyal, S. K. Sinha, K. G. Huang, and B. M. Ocko, *Phys. Rev. Lett.* **66**, 628 (1991).
- <sup>48</sup>B. M. Ocko, E. B. Sirota, M. Deutsch, E. DiMasi, S. Coburn, J. Strzalka, S. Zheng, A. Tronin, T. Gog, and C. Venkataraman, *Phys. Rev. E* **63**, 032602 (2001).
- <sup>49</sup>P. S. Pershan, A. Braslau, A. H. Weiss, and J. Als-Nielsen, *Phys. Rev. A* **35**, 4800 (1987).
- <sup>50</sup>D. T. Cromer and D. Liberman, *J. Chem. Phys.* **53**, 1891 (1970).
- <sup>51</sup>The software and the related information are available online at <http://cars9.uchicago.edu/ifeffit/>
- <sup>52</sup>S. T. Perkins, D. E. Cullen, M. H. Chen, J. H. Hubbell, J. Rathkopf, and J. Scofield, *Tables and Graphs of Atomic Subshell and Relaxation Data Derived from LLNL Evaluated Atomic Data Library (EADL) Z=1–100* (Lawrence Livermore National Laboratory, Livermore, CA, 1991).
- <sup>53</sup>G. Evans and R. F. Pettifer, *J. Appl. Crystallogr.* **34**, 82 (2001).
- <sup>54</sup>M. J. Regan, P. S. Pershan, O. M. Magnussen, B. M. Ocko, M. Deutsch, and L. E. Berman, *Phys. Rev. B* **54**, 9730 (1996).
- <sup>55</sup>O. Shpyrko, P. Huber, A. Grigoriev, P. S. Pershan, B. M. Ocko, H. Tostmann, and M. Deutsch, *Phys. Rev. B* **67**, 115405 (2003); O. Shpyrko, M. Fukuto, P. S. Pershan, B. M. Ocko, I. Kuzmenko, T. Gog, and M. Deutsch, *ibid.* **69**, 245423 (2004).
- <sup>56</sup>J. N. Israelachvili, *Intermolecular and Surface Forces* (Academic, San Diego, 1992); I. Danielewicz-Ferchmin and A. R. Ferchmin, *J. Solution Chem.* **31**, 81 (2002); J. L. Palmer and M. E. Gunter, *Am. Mineral.* **86**, 431 (2001).
- <sup>57</sup>P. S. Pershan, *Colloids Surf., A* **171**, 149 (2000).
- <sup>58</sup>E. Sloutskin, R. M. Lynden-Bell, S. Balasubramanian, and M. Deutsch, *J. Chem. Phys.* **125**, 174715 (2006).
- <sup>59</sup>O. Gang, X. Z. Wu, B. M. Ocko, E. B. Sirota, and M. Deutsch, *Phys. Rev. B* **58**, 6086 (1998).
- <sup>60</sup>S. Ramos, Ph.D. thesis University of Bristol, 2001.
- <sup>61</sup>J. Emsley, *The Elements*, 3rd ed. (Clarendon, Oxford, 1998).
- <sup>62</sup>Attempts to use the distorted crystal model (Ref. 54) to fit the experimental data yielded fits which were no better than those obtained with a monotonic, unstructured density profile of  $|\Phi(q_z)|^2=1$ .